Leveraging Stacked Intelligent Surfaces for Near-Field Localization by Using a Multi-Port Network Model

Andrea Abrardo, *Senior Member, IEEE*, Giulio Bartoli *Member, IEEE*, Alberto Toccafondi, *Senior Member, IEEE*
Marco Di Renzo, *Fellow Member, IEEE*

***Abstract*—In this paper, we leverage stacked intelligent metasurfaces (SIMs) to enable near-field localization. To this end, we employ a multi-port network model, which enables the electromagnetically consistent characterization of SIMs and is suitable for optimization as well. Near-field localization is achieved by processing the signals at a receiving array, and by exploiting the curvature of the incoming wavefront. We show how an SIM can be used to accomplish this goal. Specifically, we prove that an SIM can be optimized to perform a linear transformation that operates entirely in the electromagnetic domain, and that the proposed linear transformation of the input signal accounts for both angular and distance information simultaneously, which are required for near-field localization.**

I. Introduction

Stacked intelligent metasurface (SIM) is an innovative and recently proposed technology that is composed of a cascaded of multiple transmitting reconfigurable intelligent surfaces (T-RIS). In an SIM, each intelligent metasurface operates as a layer of a deep neural network (DNN), while each programmable meta-atom operates akin to a neuron subject to a linear input-output response, exhibiting adjustable phase and amplitude responses that can be customized to fulfill various tasks and adapt to dynamic environments [1]. Consequently, SIMs benefit from the robust representation capabilities of artificial neural networks (ANNs), the exceptional speed in electromagnetic computing, and the energy-efficient tuning attributes of reconfigurable metasurfaces.

The number of research works on SIM is rapidly increasing due to the heightened interest in the field. SIM has demonstrated its efficacy in performing beamforming in the electromagnetic domain [1] and enabling holographic multiple-input multiple-output communications without requiring many radio-frequency (RF) chains [2], [3]. Several studies also address near-field communications, such as [4], where users are equipped with multiple antennas, and [5], which takes into consideration the diffraction behavior of SIM's reconfigurable elements. Moreover, SIMs can enhance sensing performance. For instance, the estimation of the direction of arrival can be improved using SIMs, as examined in [6] and [7]. Furthermore, the role of SIMs in integrated sensing and communication (ISAC) has been evaluated in recent studies [8]–[11].

Despite the potential of SIM technology, its accurate and tractable modeling remains a considerable challenge. Existing studies utilize a simplified model that characterizes the SIM as a cascade of ideal transmit-arrays, assuming that the input signals propagate through almost decoupled inter-layer channels. Noteworthy efforts to establish more accurate models are presented in [12] and [13], based on a multiport network model. In [13], an iterative algorithm that leverages the layered architecture of SIM is introduced. This algorithm allows the optimization of SIM via a gradient descent approach, showcasing the adaptability of SIMs to perform signal processing functions directly in the electromagnetic domain.

A. Motivation and Contribution

Near-field signals emitted or received by antenna arrays depend on both angle and distance information, enabling object localization [14]. This simplifies the localization of targets compared to time of arrival or triangulation methods. SIM allows object localization in the wave domain, reducing the need for costly RF chains and digital-to-analog conversion. In this paper, we capitalize on the curvature of near-field signals, and employ the model for SIM in [13] for near-field localization. We show that an SIM can perform linear transformations entirely in the electromagnetic domain, enabling the accurate localization of objects, while reducing signal processing complexity and power consumption.

II. SIM Model

We first present the multi-port network model to characterize an SIM [13]. An SIM is a layered structure housed within a supporting box of wave-absorbing materials to minimize interference from unwanted diffraction, scattering, and environmental noise. A block diagram illustrating the architecture of the considered SIM is shown in Fig. 1.

We consider an SIM composed of Q T-RISs. Each T-RIS is composed of K unit-cells indexes by $\{1, \ldots, K\}$ where the k-th unit-cell consists of two scattering elements denoted by k and $k + K$. In a K-cell T-RIS, therefore, there are

A. Abrardo, G. Bartoli and A. Toccafondi are with the University of Siena and CNIT. Email: abrardo@unisi.it, giulio.bartoli@unisi.it, alberto.toccafondi@unisi.it.

M. Di Renzo is with Université Paris-Saclay, CNRS, CentraleSupélec, Laboratoire des Signaux et Systèmes, 3 Rue Joliot-Curie, 91192 Gif-sur-Yvette, France. (marco.di-renzo@universite-paris-saclay.fr), and with King's College London, Centre for Telecommunications Research – Department of Engineering, WC2R 2LS London, United Kingdom (marco.di_renzo@kcl.ac.uk).

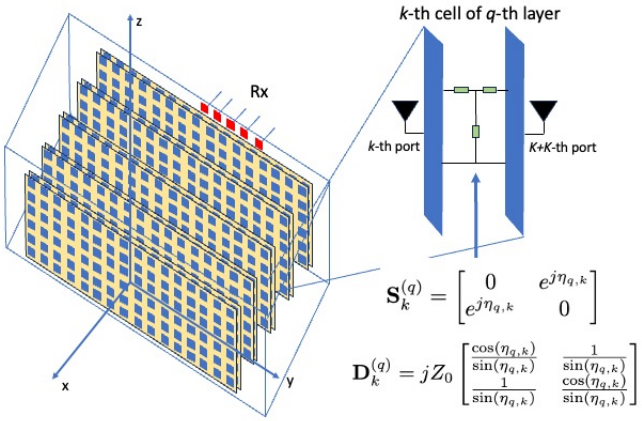

Fig. 1: SIM architecture

$2K$ scattering elements connected to a $2K$-port reconfigurable impedance network. In Fig. 1, a unit-cell of a layer of the SIM is highlighted, where the two scattering elements, k and $k+K$, are located on the left and right, respectively, and are connected to each other by a two-port linear passive network. In this case, the unit-cells are isolated, and are hence not connected to other unit-cells. This represents the simplest configuration, also known as diagonal implementation [13], which is considered in this work.

To elaborate, the SIM is modeled as a $2KQ$-port network and, as such, it can be modeled through a Z-parameter representation. Specifically, we denote by $\mathbf{Z}_{SS} \in \mathbb{C}^{2QK \times 2QK}$ the Z-parameter matrix of the SIM. With the considered parametrization, this matrix does not depend on the configuration of the impedance network driving the SIM layers, but it depends solely on the structural arrangement of the SIM, e.g., the number of unit-cells in each layer, the number of layers, the types of elements (dipoles, patches, etc.), and the distances between the layers [13]. As such, $\mathbf{Z}_{SS}$ can be calculated either analytically, for example by considering thin wire dipoles as scattering elements due to their analytical tractability [15], or with the aid of full-wave electromagnetic simulators [16]. In any case, $\mathbf{Z}_{SS}$ is assumed known in this paper. As discussed in [13], this representation allows for an electromagnetically consistent treatment of SIM, eliminating certain approximations that are implicitly made by using simplified scattering models.

As for the internal impedance network in each SIM layer, we consider diagonal T-RISs and assume that the connections between the scattering elements k and $k+K$ are modeled as linear passive two-port networks configured as ideal phase shifters. For this purpose, T-type two-port networks with purely reactive loads can be considered, which can be represented in terms of S-parameters by setting $s_{1,1}$ and $s_{2,2}$ equal to zero, and $s_{2,1} = s_{1,2} = e^{j\eta_{q,k}}$ [17]. In essence, the considered model represents an ideal setting in which the signals that go through the network are subject to a phase shift with zero attenuation. Thus, the two-port network depends on a single parameter. Denoting by $\mathbf{D}_k^{(q)} \in \mathbb{C}^{2\times 2}$ the Z-matrix representation of the k-th phase shifter of the q-th layer, we obtain [18]

$$\mathbf{D}_k^{(q)} = jZ_0 \begin{bmatrix} \frac{\cos(\eta_{q,k})}{\sin(\eta_{q,k})} & \frac{1}{\sin(\eta_{q,k})} \\ \frac{1}{\sin(\eta_{q,k})} & \frac{\cos(\eta_{q,k})}{\sin(\eta_{q,k})} \end{bmatrix}. \tag{1}$$

As shown in [13], from (1) it is possible to define the total impedance matrix $\mathbf{Z}_S(\boldsymbol{\eta}) \in \mathbb{C}^{2QK\times 2QK}$, which depends on all the KQ configurable terms $\boldsymbol{\eta} = \{\boldsymbol{\eta}_1, \ldots, \boldsymbol{\eta}_Q\}$ with $\boldsymbol{\eta}_q = \eta_{q_1}, \ldots, \eta_{q_K}$. The two matrices $\mathbf{Z}_{SS}$ and $\mathbf{Z}_S(\boldsymbol{\eta})$ allow us to represent the input-output relationship of the SIM. To elaborate, denoting by $\mathbf{x} \in \mathbb{C}^{M\times 1}$ the received vector at the output of the SIM, by $\mathbf{A} \in \mathbb{C}^{M\times K}$ the matrix representing the receiver-SIM impedance matrix, and by $\mathbf{b} \in \mathbb{C}^{K\times 1}$ the signal vector received at the SIM, we have

$$\mathbf{x} = \mathbf{h}_T(\boldsymbol{\eta}) = \mathbf{A}\mathbf{T}(\boldsymbol{\eta})\mathbf{b}. \tag{2}$$

where $\mathbf{T}(\boldsymbol{\eta}) = (\mathbf{Z}_{SS} + \mathbf{Z}_S(\boldsymbol{\eta}))^{-1}$.

A. SIM Optimization

This section summarizes the gradient descent algorithm utilized for the optimization of SIM. Further details can be found in [13]. We consider the problem of optimizing the SIM so that, given a set of I inputs $\mathbf{b}_i$, $i = 1, 2, \ldots, I$, the SIM provides an output that "closely approximates" the desired output vectors $\mathbf{x}_i \in \mathbb{C}^{M\times 1}$, $i = 1, 2, \ldots, I$. To this aim, we introduce the notation $\mathbf{h}_T^{(i)}(\boldsymbol{\eta}) = \mathbf{A}\mathbf{T}(\boldsymbol{\eta})\mathbf{b}_i$ and

$$\epsilon_i(\boldsymbol{\eta}) = \left(\mathbf{h}_T^{(i)}(\boldsymbol{\eta}) - \mathbf{x}_i\right)^H \left(\mathbf{h}_T^{(i)}(\boldsymbol{\eta}) - \mathbf{x}_i\right). \tag{3}$$

We then consider the following optimization problem:

$$\min_{\boldsymbol{\eta}} \sum_i \epsilon_i(\boldsymbol{\eta}). \tag{4}$$

To compute the gradient of $\epsilon_i(\boldsymbol{\eta})$, it is convenient to represent the transfer function $\mathbf{T}$ as composed of sub-matrices $\mathbf{T}_{i,j} \in \mathbb{C}^{K\times K}$, with $i = 1, \ldots, 2Q$ and $j = 1, \ldots, 2Q$. Hence we introduce $\mathbf{R}_q(\boldsymbol{\eta}) = \{\mathbf{T}_{2Q,2q-1}(\boldsymbol{\eta}), \mathbf{T}_{2Q,2q}(\boldsymbol{\eta})\} \in \mathbb{C}^{K\times 2K}$, and $\mathbf{S}_q(\boldsymbol{\eta}) = \left\{\mathbf{T}_{2q-1,1}^T(\boldsymbol{\eta}), \mathbf{T}_{2q,1}^T(\boldsymbol{\eta})\right\}^T \in \mathbb{C}^{2K\times K}$. As shown in [13], these matrices can be computed using an iterative procedure without the need to calculate the total matrix $\mathbf{T}$. By introducing $\mathbf{G}_{q,k}(\boldsymbol{\eta}_q) = \frac{\partial \mathbf{Z}_S^{(q)}(\boldsymbol{\eta}_q)}{\partial \eta_{q,k}} \in \mathbb{C}^{2K\times 2K}$, which is the tangent matrix of $\mathbf{Z}_S^{(q)}(\boldsymbol{\eta}_q)$ with respect to $\eta_{q,k}$, the gradient $\nabla_{\eta_{q,k}}\epsilon_i(\boldsymbol{\eta})$ with respect to the generic tunable parameter $\eta_{q,k}$ can be expressed as follows:

$$\nabla_{\eta_{q,k}}\epsilon_i(\boldsymbol{\eta}) = \frac{\partial \epsilon_i(\boldsymbol{\eta})}{\partial \eta_{q,k}} = f_{q,p}^{(i)}(\boldsymbol{\eta}) - 2\Re\left(d_{q,p}^{(i)}(\boldsymbol{\eta})\right), \tag{5}$$

where

$$\begin{aligned} d_{q,p}^{(i)}(\boldsymbol{\eta}) &= -\mathbf{x}_i^H \mathbf{A}\mathbf{R}_q(\boldsymbol{\eta})\mathbf{G}_{q,p}(\boldsymbol{\eta}_q)\mathbf{S}_q(\boldsymbol{\eta})\mathbf{b}_i \\ f_{q,p}^{(i)}(\boldsymbol{\eta}) &= -2\Re\left\{\left(\mathbf{h}_T^{(i)}(\boldsymbol{\eta})\right)^H \mathbf{A}\mathbf{R}_q(\boldsymbol{\eta})\mathbf{G}_{q,p}(\boldsymbol{\eta}_q)\mathbf{S}_q(\boldsymbol{\eta})\mathbf{b}_i\right\}. \end{aligned} \tag{6}$$

Leveraging the gradient descent algorithm, $\boldsymbol{\eta}$ can be adjusted

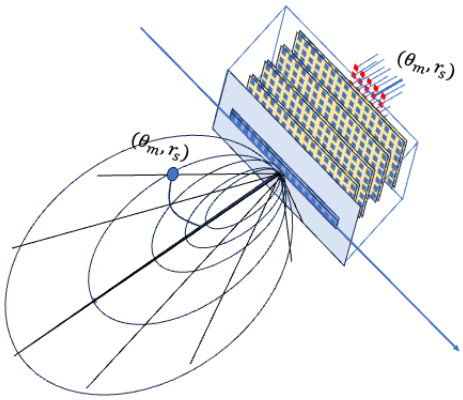

Fig. 2: Near-field scenario

iteratively according to

$$\boldsymbol{\eta}^{(t+1)} = \boldsymbol{\eta}^{(t)} - \alpha \sum_i \mathbf{f}^{(i)}\left(\boldsymbol{\eta}^{(t)}\right) - 2\Re\left(\mathbf{d}^{(i)}\left(\boldsymbol{\eta}^{(t)}\right)\right) \quad (7)$$

where α is the learning rate and $\mathbf{f}^{(i)} = \text{vec}\left(f_{q,p}^{(i)}\right) \in \mathbb{C}^{QK\times 1}$ and $\mathbf{d}^{(i)} = \text{vec}\left(d_{q,p}^{(i)}\right) \in \mathbb{C}^{QK\times 1}$.

III. Near-Field Localization

Near-field localization is realized by exploiting the curvature of the incoming wavefront. Next, we show how an SIM can be utilized to accomplish this goal.

An SIM can perform transformations that operate entirely in the electromagnetic domain. For simplicity, we assume that the geometry of the problem is two-dimensional, so that the first layer of the SIM is arranged along a single dimension, e.g., along the y-axis, and that the transmitter is located at polar coordinates (θ, r) with respect to the center of the SIM. The considered scenario is illustrated in Fig. 2, where the transmitter is located at the polar position (θ_m, r_s).

Defining by D the aperture of the SIM and by λ the wavelength, we assume to be in the Fresnel region, i.e., $r \leq \frac{2D^2}{\lambda}$, resulting in a parabolic phase profile on the receiving array. In this case, unlike classical angular-domain representations that only consider angular information, a transformation in the polar domain can be defined, as proposed in [14]. This linear transformation of the input signal accounts for the angular and distance information simultaneously.

The details of the linear transformation in the polar domain can be found in [14]. In simple terms, given $\gamma = \sin(\theta)$, it is possible to show that the incoming signals arriving from space rings defined by the curves

$$\frac{1-\gamma^2}{r} = \rho \quad (8)$$

are orthogonal provided that they are angularly spaced by at least $\Delta\gamma = 2\pi k/N$, with k being an integer and N being the dimension of the receiving array.

The obtained condition is equivalent to that obtained by a discrete Fourier transform (DFT). In other words, angular resolvability can be achieved by applying a DFT when the transmitter is positioned on the rings defined by (8), rather than being positioned on circles as in far-field channels. Fig. 2 shows some rings and the boundaries of the equispaced angles that produce orthogonal signals at the SIM's input.

The problem of distance resolvability is more complex. Considering a maximum distance $r_{\max} = \frac{D^2}{2\lambda\beta^2}$, it can be shown that, for every angle θ, the signals originating from the distances $r_s = r_{\max}\frac{1-\gamma^2}{s}$, with s being an integer, are weakly correlated if $\beta \geq 2$. In other words, for every angle, there is a set of distances for which the incoming signals are nearly orthogonal, which can then be taken as basis functions in the distance domain. The result is a transformation $\boldsymbol{\Theta} \in \mathbb{C}^{N_f N_d \times N}$ that allows for the joint identification of N_f angles and N_d distances at which the transmitter is located.

To elaborate, according to [14], such a transformation can be expressed as

$$[\boldsymbol{\Theta}]_{m(p,s),n} = e^{-j\frac{2\pi}{\lambda}\left(dl_n l_p - d^2 l_n^2 \frac{r_{\max}}{2s}\right)}. \quad (9)$$

where d is the distance between the elements of the SIM at the input layer, $l_n = \frac{2n-N-1}{2}$, with $n = 1, \ldots, N$, $l_p = \frac{2p-N_f-1}{N_f}$, with $p = 1, \ldots, N_f$, $s = 1, \ldots, N_d$ and $m(p,s) = (s-1)N_f + p$.

The transformation in (9) provides peaks corresponding to the angles

$$\theta_p = \sin^{-1}(l_p) = \sin^{-1}\left(\frac{2p - N_f - 1}{N_f}\right) \quad (10)$$

for $p = 1, \ldots, N_f$, and the distances $r(p,s) = r_{\max}\frac{1-l_p^2}{s}$, for $s = 1, \ldots, N_d$.

To implement the transformation in (9), an SIM with $N_f \times N_d$ probes at its output and N elements at its input can be considered. The SIM is to be optimized according to the following minimum square error criterion:

$$\min_{\boldsymbol{\eta}} \text{tr}\left[\left(\mathbf{AT}(\boldsymbol{\eta}) - \boldsymbol{\Theta}\right)\left(\mathbf{AT}(\boldsymbol{\eta}) - \boldsymbol{\Theta}\right)^H\right]. \quad (11)$$

Denoting the i-th column of $\mathbf{AT}(\boldsymbol{\eta})$ by $\mathbf{y}_i(\boldsymbol{\eta})$ and the i-th column of $\boldsymbol{\Theta}$ by $\mathbf{x}_i$, with $i = 1, \ldots, N$, the criterion in (11) can be rewritten as

$$\min_{\boldsymbol{\eta}} \sum_i \left(\mathbf{y}_i(\boldsymbol{\eta}) - \mathbf{x}_i\right)^H \left(\mathbf{y}_i(\boldsymbol{\eta}) - \mathbf{x}_i\right). \quad (12)$$

Since $\mathbf{y}_i(\boldsymbol{\eta}) = \mathbf{AT}(\boldsymbol{\eta})\mathbf{e}_i$, where $\mathbf{e}_i \in \mathbb{C}^{N\times 1}$ is the vector of all zeros except in the i-th position, where the entry is one, (11) can be viewed as a special case of (4).

IV. Simulation Results

We test the capability of SIM to implement the transformation in (9) assuming a carrier frequency of $f_0 = 28$ GHz. As in [13], each SIM element is a metallic dipole with a radius of $\lambda/500$ and a length of $L = 0.46\lambda$. The spacing between the dipoles is $d_y = \lambda/2$ in the y direction and $d_z = 3/4\lambda$ in the z direction. To compute the matrices $\mathbf{W}_{i,j}^{(q)} \in \mathbb{C}^{K\times K}$ for

$q = 1, 2, \ldots, Q-1$, we employ the analytical method in [15]. Moreover, the distance d_x between any two adjacent layers is set to $d_x = \lambda$, resulting in an SIM with total thickness of $(Q-1)\lambda$. The system is optimized by minimizing the error between the target $\boldsymbol{\Theta}$ in (9) and the electromagnetic response of the SIM.

We assume that the probes at the output of the SIM are dipoles identical to those of the SIM. The probes are arranged on a uniform planar array (UPA) consisting of N_d and N_f elements along the y and z axes, respectively, which are positioned at a distance of λ from the Q-th layer of the SIM. In this arrangement, the probes are aligned with the last layer of the SIM, and constitute an additional layer of the SIM with $M = N_f N_d$ elements. The first layer of the SIM consists of a uniform linear array (ULA), aligned along the y axis, with N elements, while the subsequent layers are UPAs, with N_y elements along the y axis and N_z elements along the z axis. This arrangement is depicted in Fig. 2.

The numerical results are obtained by setting $Q = 7$, $N = 64$, $N_y = 64$, $N_z = 4$, $N_f = 48$, and $N_d = 4$. Under these conditions, the aperture D of the receiving array is approximately 32 cm, which corresponds to a Fraunhofer distance of approximately 20 m. To meet the conditions of quasi-orthogonality in the r domain, $r_{\max} = 1.2$ m is considered. To simplify the optimization process, it is assumed that the transmitter is located at an angular position $\theta_{N_f-1} \leq \theta \leq \theta_{N_f+3}$, corresponding to seven degrees from the zero angle. This allows us to consider 4 values in the angular dimension, resulting in a total of 16 outputs from the SIM (4 for the angle and 4 for the distance).

To validate the effectiveness of the proposed approach to optimize the SIM, we evaluate the magnitudes of the responses of all the probes, assuming the transmitter positioned on a set of points defined by the angles $\theta_{N_f-1} \leq \theta \leq \theta_{N_f-3}$ and by the distances $\frac{r_{\max}}{N_f} \leq r \leq r_{\max}$. The results are shown in Figs. 3 and 4. Fig. 3 displays the responses of the first row of the SIM output as a function of θ for $r = r_{\max}$, while Fig. 4 shows the responses of the first column of the SIM output as a function of r for $\theta = 0$. The responses of different probes are represented by different colors, showing that a single probe attains a peak and the others are almost zero. The peak corresponds to the pairs of angle/distance that can be resolved by the SIM. The dashed and solid lines represent the SIM response and the ideal response in (9), respectively. We see that the response of the SIM is nearly overlapping with the target response, demonstrating the effectiveness of the proposed approach.

In Fig. 5, we show the Cramer-Rao bound (expressed in meters) of the estimated position of the transmitter, assuming that it is located within the spatial region bounded by the angular and distance spreads depicted in Figs. 3 and 4, respectively. The Cramer-Rao bound is calculated based on the simulated output of the SIM, assuming an additive white Gaussian noise with a noise temperature of 1000 Kelvin and a bandwidth of 100 kHz. The Cramer-Rao bound calculation employs Schur's complement to consider only the phase profile of the received signal at the SIM input, treating the signal amplitude and absolute phase as unknown nuisance parameters. As expected, the Cramer-Rao bound increases with the distance due to reduced received power. The results obtained highlight the potential of SIM for near-field localization in the electromagnetic domain.

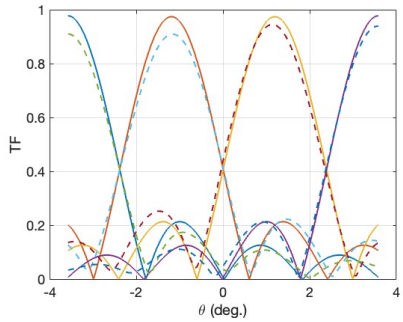

Fig. 3: Angular response: the responses of different probes are illustrated using solid and dashed lines for the SIM and target responses in (9), respectively.

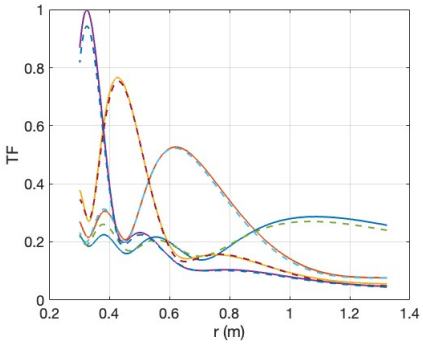

Fig. 4: Distance response: the responses of different probes are illustrated using solid and dashed lines for the SIM and target responses in (9), respectively.

V. Conclusion

In this work, we considered a comprehensive multiport network model for the optimization of SIM. By leveraging this model, we have developed an algorithm for near-field localization that operates entirely in the wave domain. The obtained results highlight the good performance attained by SIM at a low complexity due to the wave-domain processing.

Acknowledgments

The work of A. Abrardo was supported by the 6G SHINE EU project and by the the Italian National Recovery and Resilience Plan (NRRP) of NextGenerationEU, partnership on "Telecommunications of the Future". The work of A. Toccafondi was supported by the EU – NextGenerationEU under the National Recovery and Resilience Plan (PNRR), through the Cascade Funding Call of Spoke 7 'GREEN AND SMART ENVIRONMENTS', within the project 'Smart Metasurfaces Advancing Radio Technology (SMART)'. The work of M. Di

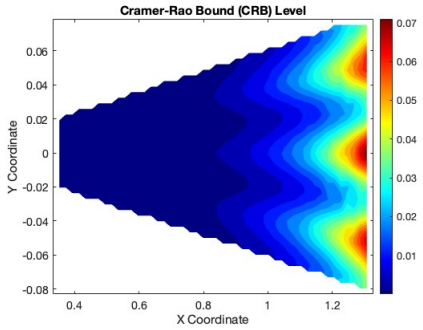

Fig. 5: Cramer-Rao bound of 2D positioning obtained with the SIM

Renzo was supported in part by the European Union through the Horizon Europe project COVER under grant agreement number 101086228, the Horizon Europe project UNITE under grant agreement number 101129618, the Horizon Europe project INSTINCT under grant agreement number 101139161, and the Horizon Europe project TWIN6G under grant agreement number 101182794, as well as by the Agence Nationale de la Recherche (ANR) through the France 2030 project ANR-PEPR Networks of the Future under grant agreement NF-YACARI 22-PEFT-0005, and by the CHIST-ERA project PASSIONATE under grant agreements CHIST-ERA-22-WAI-04 and ANR-23-CHR4-0003-01.

REFERENCES

[1] M. Di Renzo, "State of the art on stacked intelligent metasurfaces: Communication, sensing and computing in the wave domain," 2025. [Online]. Available: https://doi.org/10.48550/arXiv.2411.19687

[2] N. U. Hassan, J. An, M. Di Renzo, M. Debbah, and C. Yuen, "Efficient beamforming and radiation pattern control using stacked intelligent metasurfaces," *IEEE Open J. Commun. Soc.*, vol. 5, pp. 599–611, 2024. [Online]. Available: https://doi.org/10.1109/OJCOMS.2023.3349155

[3] J. An, C. Xu, D. W. K. Ng, G. C. Alexandropoulos, C. Huang, C. Yuen, and L. Hanzo, "Stacked intelligent metasurfaces for efficient holographic MIMO communications in 6G," *IEEE J. Sel. Areas Commun.*, vol. 41, no. 8, pp. 2380–2396, 2023. [Online]. Available: https://doi.org/10.1109/JSAC.2023.3288261

[4] A. K. Papazafeiropoulos, P. Kourtessis, S. Chatzinotas, D. I. Kaklamani, and I. S. Venieris, "Near-field beamforming for stacked intelligent metasurfaces-assisted MIMO networks," *IEEE Wirel. Commun. Lett.*, vol. 13, no. 11, pp. 3035–3039, 2024. [Online]. Available: https://doi.org/10.1109/LWC.2024.3438840

[5] X. Jia, J. An, H. Liu, L. Gan, M. Di Renzo, M. Debbah, and C. Yuen, "Stacked intelligent metasurface enabled near-field multiuser beamfocusing in the wave domain," in *99th IEEE Vehicular Technology Conference, VTC Spring 2024, Singapore, June 24-27, 2024*. IEEE, 2024, pp. 1–5. [Online]. Available: https://doi.org/10.1109/VTC2024-Spring62846.2024.10683447

[6] J. An, C. Yuen, Y. L. Guan, M. Di Renzo, M. Debbah, H. V. Poor, and L. Hanzo, "Stacked intelligent metasurface performs a 2d DFT in the wave domain for DOA estimation," in *IEEE International Conference on Communications, ICC 2024, Denver, CO, USA, June 9-13, 2024*. IEEE, 2024, pp. 3445–3451. [Online]. Available: https://doi.org/10.1109/ICC51166.2024.10622963

[7] ——, "Two-dimensional direction-of-arrival estimation using stacked intelligent metasurfaces," *IEEE J. Sel. Areas Commun.*, vol. 42, no. 10, pp. 2786–2802, 2024. [Online]. Available: https://doi.org/10.1109/JSAC.2024.3414613

[8] H. Niu, J. An, A. K. Papazafeiropoulos, L. Gan, S. Chatzinotas, and M. Debbah, "Stacked intelligent metasurfaces for integrated sensing and communications," *IEEE Wirel. Commun. Lett.*, vol. 13, no. 10, pp. 2807–2811, 2024. [Online]. Available: https://doi.org/10.1109/LWC.2024.3447272

[9] S. Li, F. Zhang, T. Mao, R. Na, Z. Wang, and G. K. Karagiannidis, "Transmit beamforming design for ISAC with stacked intelligent metasurfaces," *IEEE Transactions on Vehicular Technology*, pp. 1–6, 2024.

[10] C. Pei, K. Huang, L. Jin, X. Xu, Y. Zhou, and Y. Guo, "Stacked intelligent metasurfaces assisted integrated-sensing-and-resistance anti jamming," *IEEE Communications Letters*, pp. 1–1, 2024.

[11] Z. Wang, H. Liu, J. Zhang, R. Xiong, K. Wan, X. Qian, M. Di Renzo, and R. C. Qiu, "Multi-user ISAC through stacked intelligent metasurfaces: New algorithms and experiments," in *2024 IEEE Global Communications Conference (GLOBECOM): 8–12 December 2024, Cape Town, South Africa*, Cape Town, SA, 2024.

[12] M. Nerini and B. Clerckx, "Physically consistent modeling of stacked intelligent metasurfaces implemented with beyond diagonal RIS," *IEEE Communications Letters*, vol. 28, no. 7, pp. 1693–1697, 2024.

[13] A. Abrardo, G. Bartoli, and A. Toccafondi, "A novel comprehensive multiport network model for stacked intelligent metasurfaces (SIM) characterization and optimization," 2025. [Online]. Available: https://arxiv.org/abs/2501.02597

[14] M. Cui and L. Dai, "Channel estimation for extremely large-scale MIMO: Far-field or near-field?" *IEEE Transactions on Communications*, vol. 70, no. 4, pp. 2663–2677, 2022.

[15] G. Gradoni and M. Di Renzo, "End-to-end mutual coupling aware communication model for reconfigurable intelligent surfaces: An electromagnetic-compliant approach based on mutual impedances," *IEEE Wireless Communications Letters*, vol. 10, no. 5, pp. 938–942, 2021.

[16] A. Abrardo, A. Toccafondi, and M. Di Renzo, "Design of reconfigurable intelligent surfaces by using S-parameter multiport network theory – Optimization and full-wave validation," *IEEE Transactions on Wireless Communications*, vol. 23, no. 11, pp. 17 084–17 102, 2024.

[17] I. Bahl and P. Bhartia, *Microwave Solid State Circuit Design*, 2nd ed. John Wiley & Sons, Inc., 2003.

[18] D. M. Pozar, *Microwave Engineering*, 4th ed. John Wiley & Sons, Inc., 2011.